



This is a repository copy of *X-ray mapping in a scanning transmission electron microscope of InGaAs quantum dots with embedded fractional monolayers of aluminium.*

White Rose Research Online URL for this paper:
<https://eprints.whiterose.ac.uk/160074/>

Version: Published Version

Article:

Walther, T. orcid.org/0000-0003-3571-6263, Nutter, J., Reithmaier, J.P. et al. (1 more author) (2020) X-ray mapping in a scanning transmission electron microscope of InGaAs quantum dots with embedded fractional monolayers of aluminium. *Semiconductor Science and Technology*, 35 (8). 084001. ISSN 0268-1242

<https://doi.org/10.1088/1361-6641/ab8c52>

Reuse

This article is distributed under the terms of the Creative Commons Attribution (CC BY) licence. This licence allows you to distribute, remix, tweak, and build upon the work, even commercially, as long as you credit the authors for the original work. More information and the full terms of the licence here:
<https://creativecommons.org/licenses/>

Takedown

If you consider content in White Rose Research Online to be in breach of UK law, please notify us by emailing eprints@whiterose.ac.uk including the URL of the record and the reason for the withdrawal request.



eprints@whiterose.ac.uk
<https://eprints.whiterose.ac.uk/>

ACCEPTED MANUSCRIPT • OPEN ACCESS

X-ray mapping in a scanning transmission electron microscope of InGaAs quantum dots with embedded fractional monolayers of aluminium

To cite this article before publication: Thomas Walther *et al* 2020 *Semicond. Sci. Technol.* in press <https://doi.org/10.1088/1361-6641/ab8c52>

Manuscript version: Accepted Manuscript

Accepted Manuscript is “the version of the article accepted for publication including all changes made as a result of the peer review process, and which may also include the addition to the article by IOP Publishing of a header, an article ID, a cover sheet and/or an ‘Accepted Manuscript’ watermark, but excluding any other editing, typesetting or other changes made by IOP Publishing and/or its licensors”

This Accepted Manuscript is © 2020 The Author(s). Published by IOP Publishing Ltd..

As the Version of Record of this article is going to be / has been published on a gold open access basis under a CC BY 3.0 licence, this Accepted Manuscript is available for reuse under a CC BY 3.0 licence immediately.

Everyone is permitted to use all or part of the original content in this article, provided that they adhere to all the terms of the licence <https://creativecommons.org/licenses/by/3.0>

Although reasonable endeavours have been taken to obtain all necessary permissions from third parties to include their copyrighted content within this article, their full citation and copyright line may not be present in this Accepted Manuscript version. Before using any content from this article, please refer to the Version of Record on IOPscience once published for full citation and copyright details, as permissions may be required. All third party content is fully copyright protected and is not published on a gold open access basis under a CC BY licence, unless that is specifically stated in the figure caption in the Version of Record.

View the [article online](#) for updates and enhancements.

X-ray mapping in a scanning transmission electron microscope of InGaAs quantum dots with embedded fractional monolayers of aluminium

T Walther^{1*}, J Nutter², J.P. Reithmaier³ and E.-M. Pavelescu^{4*}

¹ Kroto Centre for High Resolution Imaging and Analysis, Department of Electronic and Electrical Engineering, Mappin Building

² The Henry Royce Institute and Department of Materials Science and Engineering, University of Sheffield, Sir Robert Hadfield Building

^{1,2} both: University of Sheffield, Mappin Street, Sheffield S1 3JD, UK

³ Technological Physics Department, Kassel University, Heinrich Plett Str. 40, 34132 Kassel, Germany

⁴ National Institute for R&D in Microtechnologies, 126A Erou Iancu Nicolae, 077190 Voluntari, and Hyperion University, 169 Calea Calarasilor, 030615 Bucharest, Romania

* Corresponding authors' e-mails: t.walther@sheffield.ac.uk; emil.pavelescu@imt.ro

Abstract:

We investigate AlGaAs/GaAs superlattices as well as InGaAs/GaAs quantum wells (QWs) and epitaxial quantum dots (QDs) where during the molecular beam epitaxy of InGaAs QDs the aluminium flux cell was opened briefly to incorporate fractional monolayers of Al into the InGaAs. We show that X-ray mapping with a large collection angle is capable to detect 0.3-0.4 fractional Al monolayers with a resolution of just under 1nm.

1. Introduction

Energy-dispersive X-ray spectroscopy (EDXS) in a scanning transmission electron microscope (STEM) allows the direct chemical detection of all elements heavier than beryllium (or lithium, depending on detector entrance window type and spectrometer

1
2
3 resolution) by local spectroscopy and compositional mapping at high spatial
4 resolution. Many studies have been conducted over decades to improve quantification
5 accuracy or spatial resolution.
6

7 Quantification in (S)TEM depends on the knowledge of the ionisation cross-sections
8 of the chemical elements as a function of their atomic number (Z -effect) that was
9 already modelled by Bethe in 1930 [1] and corrections for both absorption (A) of the
10 X-rays in the specimen [2] and mutual fluorescence (F) between different X-ray lines
11 [3]. This ZAF correction is still the basis of all commercial quantification procedures
12 while new self-consistent iterative approaches such as the zeta-factor method [4] and
13 thickness dependent k^* factors [5] have also recently been developed. Visibility of
14 atomic lattice planes in X-ray maps has been reported after the incorporation of
15 multiple X-ray detectors in transmission electron microscopes but only in rare cases
16 of very thin non-periodic test structures [6-8] atomic resolution could really be
17 verified. The corresponding maps were often too noisy for further quantification.
18

19 For semiconductor nanostructures embedded within or placed on top of thin foil
20 specimens, additional geometrical corrections may be needed to evaluate line
21 intensity ratios [9-13].
22

23 The University of Sheffield has recently acquired and installed a JEOL JEM-F200
24 cold field emission STEM with double windowless solid-state drift (SDD) detectors
25 that yield X-ray collection angles of 1.0 and 0.7 srad (≈ 1.7 srad in combination). This
26 improves the statistics of X-ray mapping over the previous ultrathin-window Si:Li
27 detectors with 0.12srad (JEOL 2010F at 197kV) and 0.17rad (JEOL Z3100 R005 at
28 300kV) by an order of magnitude, enabling the detection and quantification of the
29 atomic occupancy of semiconducting thin films consisting of single monolayers.
30 Analysing the digital X-ray maps acquired with the JEOL Analysis Station software
31 we highlight the improved performance for quantitative X-ray mapping and profiling
32 but also problems related to spurious background signals and lack of valid k -factors.
33
34
35
36
37
38
39
40

41 **2. Experimental**

42 **2.1 Epitaxial thin film growth**

43 The motivation for this work is based on earlier results by other groups who showed
44 that the optical emission of epitaxial InGaAs QDs sandwiched between GaAs barriers
45 can be tuned by replacing the GaAs below the QDs by either AlAs [14] or
46 (InAlGa)As [15], or the GaAs cap on top by AlAs [16], or both lower and upper
47 barriers by AlAs [17]. Here, we tried to incorporate ultra-thin AlAs layers *directly*
48 *within* the InAs QDs.
49

50 The samples investigated in this work were grown on an n-type GaAs (001) substrate
51 using a Varian Gen II solid-source molecular-beam epitaxy reactor. They resemble
52 the central part of a laser structure and consist of an (Al)InGaAs-based active region
53 surrounded by GaAs barriers, waveguide-like AlGaAs/GaAs superlattices and
54 AlGaAs claddings. The growth temperature of the claddings and waveguide layers
55 was 620 °C, while a lower temperature of 590 °C was used for the barriers. The active
56
57
58
59
60

1
2
3 region was grown at 490 °C. Two samples were grown and labeled A527 and A558.
4 The active region of sample A527 consists of InAlGaAs QDs deposited as 7
5 individual repeats of alternating 0.124 nm $\text{In}_{0.14}\text{Al}_{0.28}\text{Ga}_{0.58}\text{As}$ followed by 0.112 nm
6 InAs. The total nominal Al content deposited corresponded to 0.24nm or 0.86
7 monolayer (ML) of the group III sub-lattice. The GaAs barriers were nominally 10
8 nm thick and growth interruptions of 90 s for change in growth temperature were
9 introduced after the growth of the first 7 nm of the bottom barrier and the growth of
10 first 3 nm of the top barrier. The waveguide-like superlattices consist of 8 pairs of 2.4
11 nm GaAs followed by 2 nm $\text{Al}_{0.33}\text{Ga}_{0.67}\text{As}$, surrounding the barriers, and 9 pairs of 1.7
12 nm GaAs and 2 nm $\text{Al}_{0.33}\text{Ga}_{0.67}\text{As}$. $\text{Al}_{0.33}\text{Ga}_{0.67}\text{As}$ cladding layers surround the
13 superlattices. Another structure which leaves QDs uncovered on the free surface was
14 repeated on top of the last AlGaAs cladding layer for giving access to the QDs
15 morphology by AFM or SEM. The claddings, the superlattice waveguides and the
16 barriers of sample A558 were similar in thickness, composition and growth
17 temperature to those of the A527 sample, except for the active region. This consisted
18 of a 7 nm $\text{In}_{0.25}\text{Ga}_{0.75}\text{As}$ quantum well deposited after the growth of the first 10 nm
19 GaAs barrier, followed by a 2 nm GaAs spacer layer on top of which $\text{In}_{0.6}\text{Ga}_{0.4}\text{As}$
20 QDs with insertion of a very thin Al layer were deposited before the top 10 nm barrier
21 was eventually grown. The QDs were grown by depositing 9 individual layers of
22 equal thickness (0.2 nm) of material, as thus: first we deposited 2 layers consisting of
23 0.1 nm $\text{In}_{0.2}\text{Ga}_{0.8}\text{As}$ and 0.1 nm of InAs each, then 1 repeat of 0.12 nm $\text{In}_{0.34}\text{Al}_{0.66}\text{As}$
24 and 0.08 nm InAs, then another 6 repeats similar to the first 2. As in the case of A527,
25 the last 3nm of the bottom GaAs barrier, the QW, the GaAs spacer, the QDs and the
26 first 3 nm of the top GaAs barrier were all grown at the same temperature of 490 °C.
27 An overview of both structures is presented in Table 1.
28
29
30
31
32
33
34
35
36
37
38
39
40
41
42
43
44
45
46
47
48
49
50
51
52
53
54
55
56
57
58
59
60

sample	A527	both	A558
thick- ness [nm]	material		
1.65	InGaAs + Al	QD	QD
2	GaAs	-	spacer
7	InGaAs	-	QW
10	GaAs	barrier	
2.4/2.0	GaAs / AlGaAs	superlattice 8x	
1.7/2.0	GaAs / AlGaAs	superlattice 9x	
20	AlGaAs	cladding	
1.7/2.0	GaAs / AlGaAs	superlattice 9x	
2.4/2.0	GaAs / AlGaAs	superlattice 8x	
10	GaAs	barrier	
1.65	InGaAs + Al	QD	QD
2	GaAs	-	spacer
7	InGaAs	-	QW
10	GaAs	barrier	
2.4/2.0	GaAs / AlGaAs	superlattice 8x	
1.7/2.0	GaAs / AlGaAs	superlattice 9x	
20	AlGaAs	cladding	
150	GaAs	buffer	
	GaAs	substrate	

Table 1: schematic of both samples. QD = quantum dot, QW = quantum well.

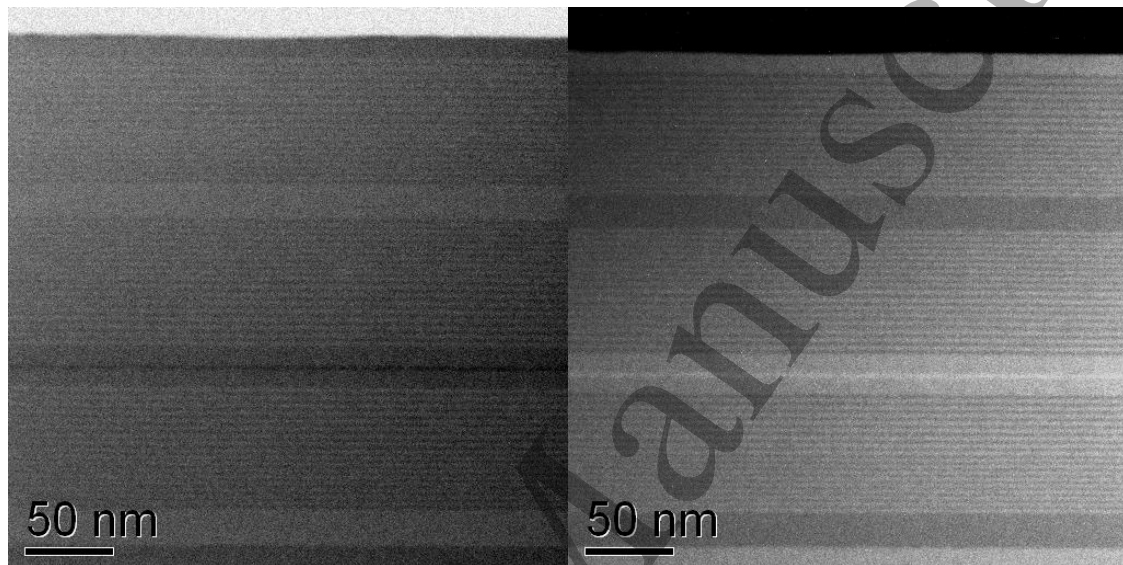
2.2 Specimen preparation for electron microscopy

Electron transparent thin foils were prepared by glueing together wafer pieces using two-component epoxy glue, cutting with a diamond impregnated wire saw along <110> directions, grinding by SiC abrasive and polishing with 3 μ m and finally 1 μ m diamond paste. The cross-sections were then argon ion milled in either a Technoorg Linda IV3 under liquid nitrogen cooling or a Gatan PIPS ion mill, at angles of $\sim 5^\circ$ and energies of initially 4keV until perforation, then 2keV and finally 0.5keV.

2.3 STEM characterization

The scanning transmission electron microscopy (STEM) imaging was performed in two instruments: a JEOL 2010F (Schottky field emitter, 197kV, 10mrad semi-angle of

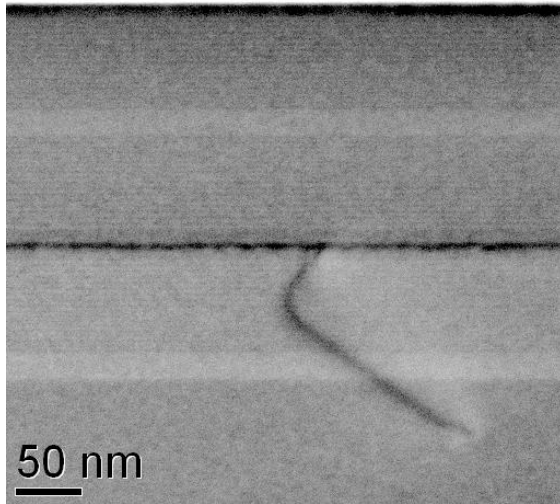
1
2
3 beam convergence, 0.3nm probe, ~20pA current at nominal spot size M, 55–170mrad
4 collection angle in high-angle annular dark field (HAADF) mode, Si:Li PentaFET X-
5 ray detector with 0.12srad collection angle and ultrathin window) and a JEOL F200
6 (cold field emitter, 200kV, 20mrad semi-angle of convergence, 0.16nm probe,
7 ~100pA current at nominal spot size 6, 45–165 mrad HAADF collection angle,
8 1.7srad windowless double silicon drift detectors for X-rays). All images and maps
9 were acquired with the layers oriented vertical to minimize both scan and drift
10 artifacts and are displayed in the following rotated by 90° so that the growth direction
11 points upwards.
12
13
14
15



34
35 **Figure 1:** Bright field (BF, left) and annular dark field (ADF, right) images of sample
36 A527. Overview of the layer stack at 200kX. Visible are the outermost 19nm AlGaAs
37 cladding layers (dark in ADF), several 32nm and 34nm thick 8×AlGaAs/GaAs
38 superlattices and two 8nm and 10nm GaAs barriers that sandwich a ~3nm thin central
39 InGaAs layer (bright in ADF).
40

41
42 The images in figure 1 of sample A527 show layers as described in the nominal stack
43 design, with apparently perfect GaAs/AlGaAs superlattices but two deviations from
44 the nominal design: the AlGaAs cladding layers are only 19nm wide, and the
45 (In,Al,Ga)As has formed a continuous ~3nm thin slightly corrugated quantum well
46 with slight lateral variations, however, as the specimen foil thickness is relatively
47 large, it is not possible to reliably distinguish a continuous quantum well from a series
48 of dots in projection. In some cases dislocations emanating from the InAlGaAs layer
49 have been found (cf. figure 2). The surface of the wafer could not be analysed in
50 detail here and no clear evidence of any quantum dots there was found. In ADF mode
51 the intensity depends almost linearly on the specimen thickness and approximately
52 quadratically on the average atomic number (Z) of the material, and this is often
53 referred to as Z -contrast [18]. Hence, indium rich layers in (Al,Ga,In)As appear bright
54 in ADF, and the square root of their ADF intensity is a signal approximately
55 proportional to the local chemical composition and to the sample thickness [19] if the
56
57
58
59
60

1
2
3 inner collection angle is sufficiently large [20].
4
5
6



23 **Figure 2:** BF image of sample A527 at 150kX. The sample is thinner here and clearly
24 shows strain modulations characteristic of strained quantum dots, as well as a
25 dislocation line emanating from the strained InGaAs quantum dot layer.
26

27
28 The dislocation shown in figure 2 runs through the superlattices and cladding layer
29 into the buffer region where it terminates on the specimen surface. As buffer, cladding
30 layer and superlattices are all made of AlGaAs lattice matched to GaAs, while the
31 InGaAs that has a larger lattice constant is compressively strained, we can conclude
32 that if the dislocation relaxes strain it is likely to have generated at a quantum dot.
33
34
35
36
37
38
39
40
41
42
43
44
45
46
47
48
49
50
51
52
53
54
55
56
57
58
59
60

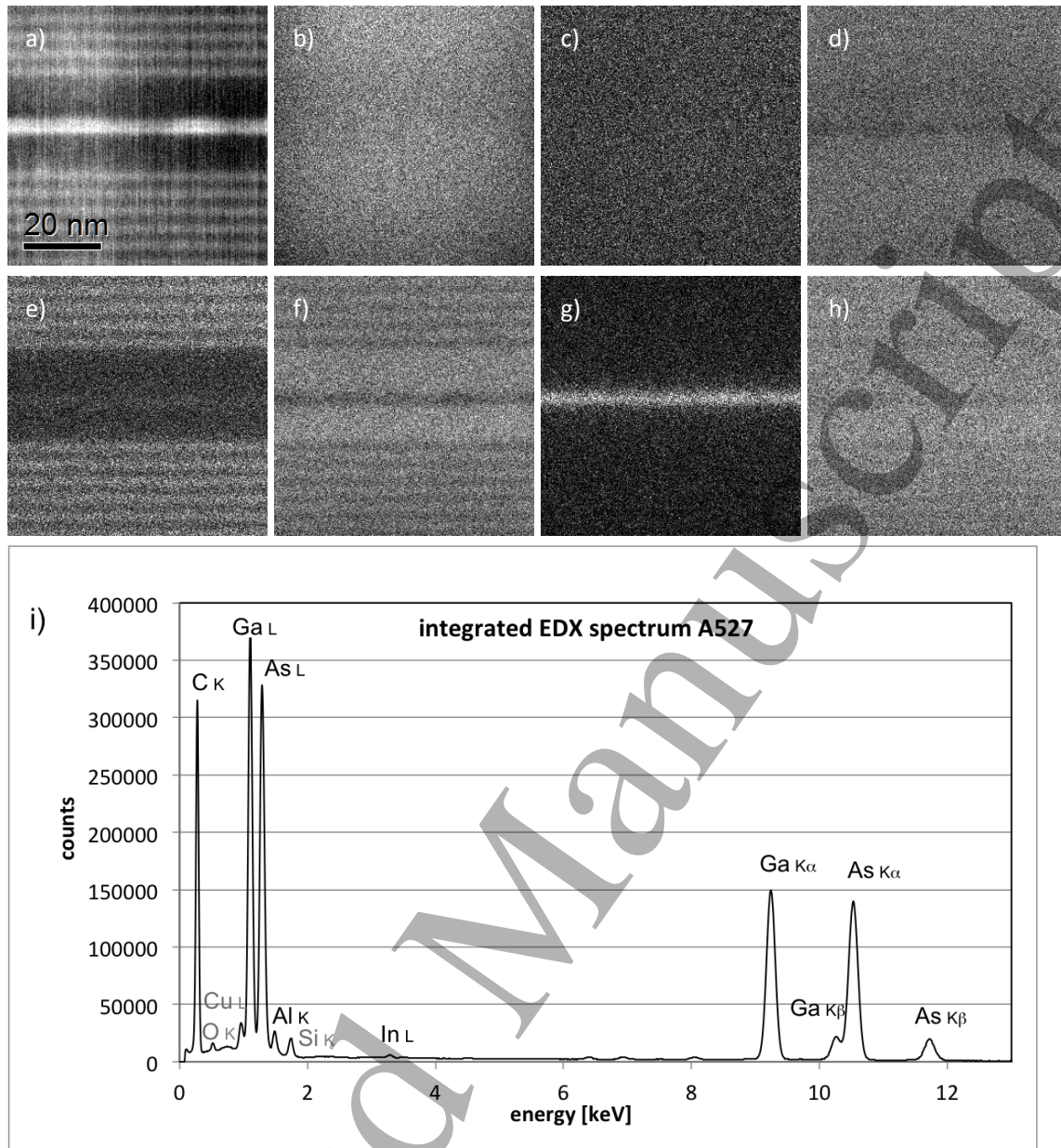


Figure 3: ADF image (a) and X-ray maps recorded of sample A527 at 3MX, 67 nm field of view, 0.26nm/pixel sampling. 256^2 pixels, 0.16nm probe, 0.1nA, 0.2ms dwell time, 52 sweeps with drift correction for 12 minutes, 13kcps from detector #1 and 15kcps from detector #2. The maps show the net signals of C_K (b), O_K (c), As_K (d), Al_K (e), Ga_K (f), In_L (g) and the sum of all group III elements (h=e+f+g). i) integrated X-ray spectrum from figure 3a) on linear scale.

The X-ray maps in figure 3b-f depict the spatial distribution of elements in a specimen estimated from tilting experiments to be ~ 30 nm thin (for details see section 3). The indium rich QW/QD layer in the centre, surrounded by first GaAs barriers and then the AlGaAs/GaAs superlattices, is visible, as well as, very faintly in figure 3e, an enrichment of Al approximately at the same height where a dark band can be seen running through the InGaAs layer in figure 3a. The nearly featureless maps of As in figure 3d and of Al+Ga+In in figure 3g are very similar and indicate that the effect of

different relative fluorescence yields of the various X-ray lines (often referred to as k -factors [21]) deviate from unity by only a few % relative and so are negligible here. Table 2 shows that maps of elements not in the specimen of sample A527 but present in the specimen support (Cu), or specimen holder and objective lens (Fe, Co) yield featureless maps of 1.3-1.6 counts per pixel on average. O from surface contamination (2.7 ± 1.6 counts) and Si from the detector material itself (3.5 ± 1.8 counts) are slightly higher but also close to the overall detection limit and reveal no structure. Whether the pervasive background signal of ~ 1.3 counts in all maps is due to real bremsstrahlung reaching the X-ray detectors or a detector artifact, is still under investigation, however, it has been shown previously that for accurate quantification it is important to subtract off even such low background signals using fractional counts [22]. Figure 4 compares profiles of Al and In (divided by the sum of Al+Ga+In to normalize with respect to occupancy of the group III sub-lattice) without and with an average of 1.3 counts subtracted from each map.

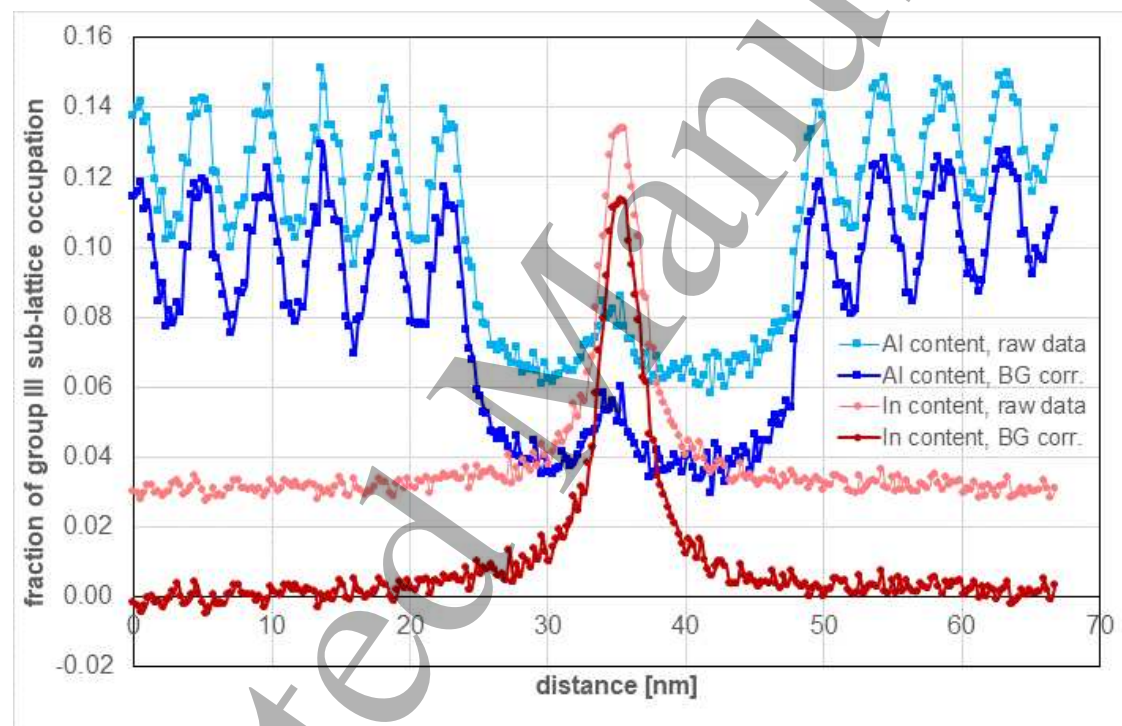


Figure 4: line profiles of the ratios of the X-ray maps of Al/(Al+Ga+In) and In/(Al+Ga+In) for sample A527 without any background correction (raw data) and after 1.3 counts subtracted from each map prior to ratio calculation (BG corrected). Neglecting k -factors for X-ray fluorescence and absorption, these yield only approximate values of the corresponding fractional occupancies of the group III sub-lattice at ~ 1 nm resolution. Note the InGaAs QD layer and the local Al increase by ~ 0.02 in the centre are displaced laterally by two data points, i.e. 0.5 nm (approximately a unit cell).

The Al content of the 4.5 nm period superlattice varies by only about $\Delta y_{\text{Al}} = 0.08$ (between $\text{Al}_{0.07}\text{Ga}_{0.93}\text{As}$ and $\text{Al}_{0.15}\text{Ga}_{0.85}\text{As}$, depending on background removal) and is

thus much lower than the nominal Al content of the barrier layers. Also, the ~ 10 and ~ 12 nm wide layers around the quantum dots layer appear to be not pure GaAs but AlGaAs with a low Al content of 0.04 ± 0.01 , with a slight local increase by 0.02 - 0.03 near the lower side of the InGaAs. This bump amounts to an additional Al coverage of 0.3 equivalent monolayers when integrated above the background level of 0.035 . The quantum dot layer itself has a maximum indium content of $x_{\text{In}} = 0.12 \pm 0.02$, again lower than nominal.

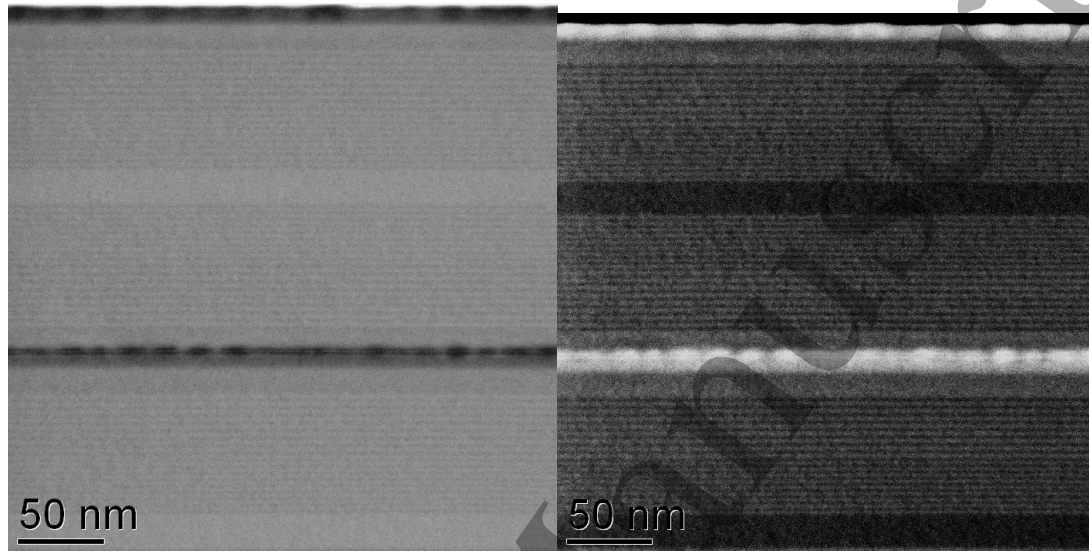


Figure 5: BF (left) and ADF (right) images of sample A558. Overview of the layer stack at 200kX . The 19nm AlGaAs cladding layers (dark in ADF) and 32nm and 34nm AlGaAs/GaAs superlattices are as in the other sample. The two GaAs barriers are 14nm and 9nm thin; the central InGaAs (bright in ADF) now consists of clearly two layers, a flat InGaAs quantum well (QW) and a quantum dot (QD) layer atop.

The images in figure 5 are from sample A558 and again show that the AlGaAs cladding layers are $\sim 19\text{nm}$ thick, the lower GaAs layer is 15nm , the middle GaAs 1nm and the top 12nm thick. The lower $\text{In}_x\text{Ga}_{1-x}\text{As}$ quantum well (nominal $x_{\text{In}} = 0.25$) in the central stack is $\sim 7\text{nm}$ thick as specified but shows a significant In segregation towards its top, yielding an indium concentration close to that of the upper In(Al)GaAs layer (nominal $x_{\text{In}} = 0.60$). Both In(Al)GaAs layers exhibit strong lateral contrast modulations which are correlated between the lower InGaAs and the upper In(Al)GaAs layers, indicating a degree of strain coupling. In the top In(Al)GaAs layer of the central stack quantum dots are now clearly visible, in line with what is expected from Stranski-Krastanow growth of InGaAs [23]. Near the free surface, a rather diffuse and slightly corrugated In(Al)GaAs layer has been formed where the intended quantum dots are clearly less well developed. The sample has also been studied by X-ray mapping as the one before, and results are shown in figures 7 and 8. Again, an increase of the Al signal under the InGaAs is found; its integral above the background level of ~ 0.06 amounts to 0.4ML half of which is located directly under the InGaAs QD while the other half appears to be more spread out.

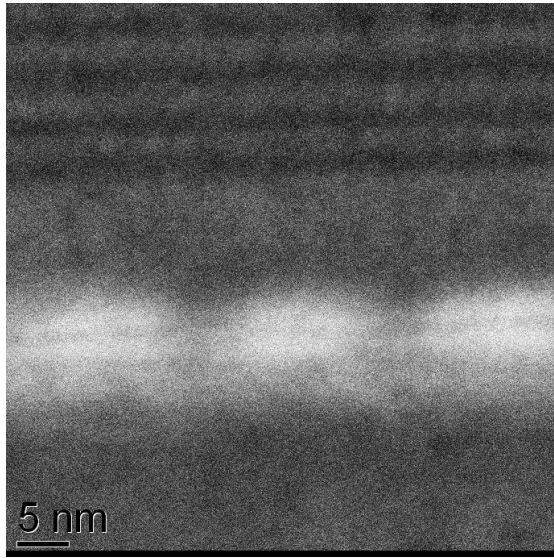


Figure 6: ADF image of sample A558 at 1MX. The InGaAs layer is clearly structured, with a 5-8nm quantum well at the bottom, followed by ~5nm high quantum dots that have a dark line running approximately through their centres (which figure 7 confirms is due to Al incorporation).

Accepted Manuscript

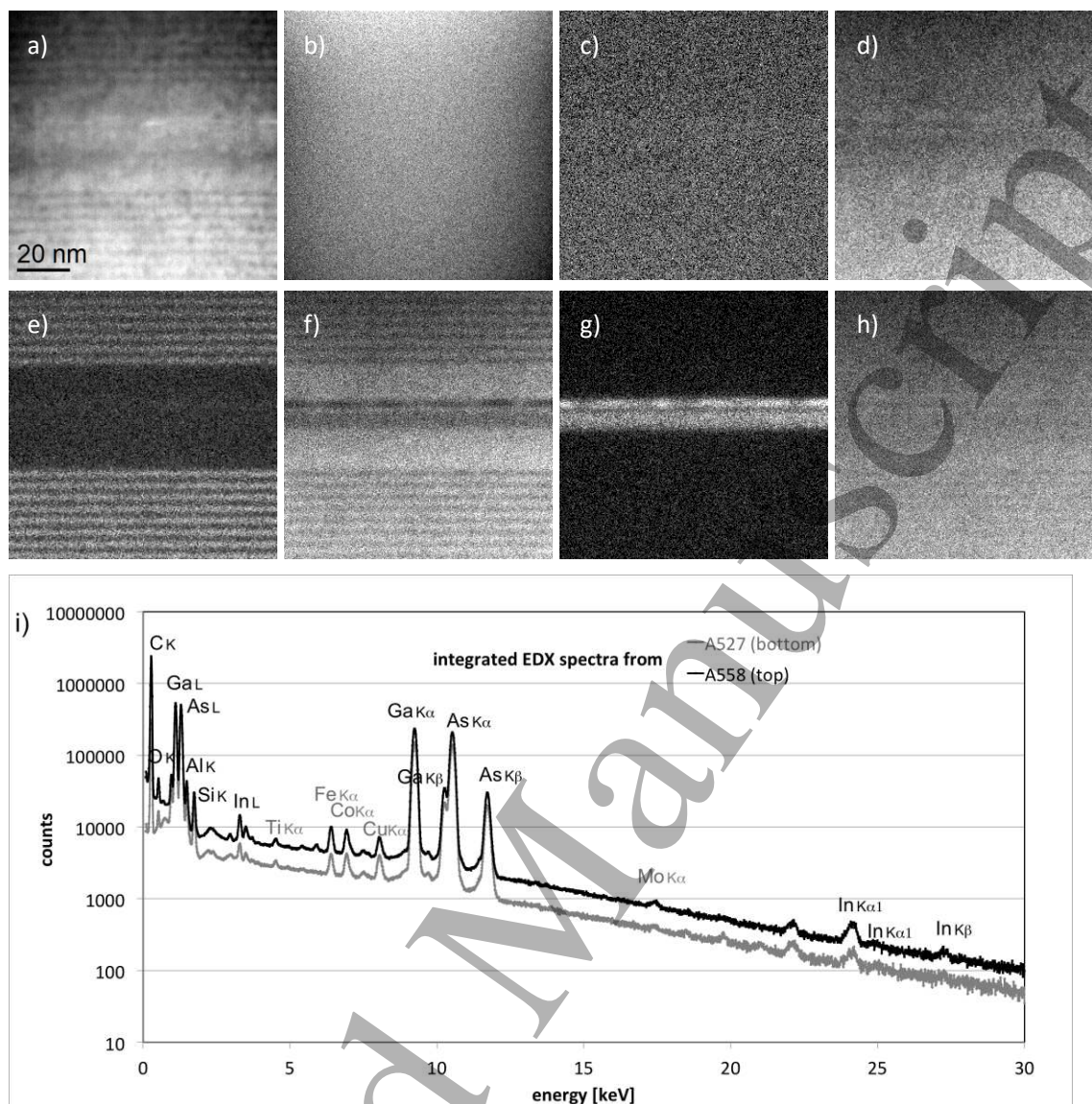


Figure 7: ADF image (a) and X-ray maps of A558 recorded at 2MX, 100 nm field of view, 0.195nm/pixel. 512^2 pixels (2x binned to 256^2 pixels at 0.39nm/pixel), 0.16nm probe (spot size 6), 0.1nA, 0.2 ms dwell time, 61 sweeps with drift correction in 53 minutes, 4kcps from detector #1 and 6kcps from detector #2. The maps show the net signals of C_K (b), O_K (c), As_K (d), Al_K (e), Ga_K (f), In_L (g) and the sum of all group III elements (h=e+f+g). The quantum dots are better visible in (g) than in (a) because this sample is very thin. i) integrated X-ray spectra from areas shown in figures 7a) and 3a) on logarithmic scale.

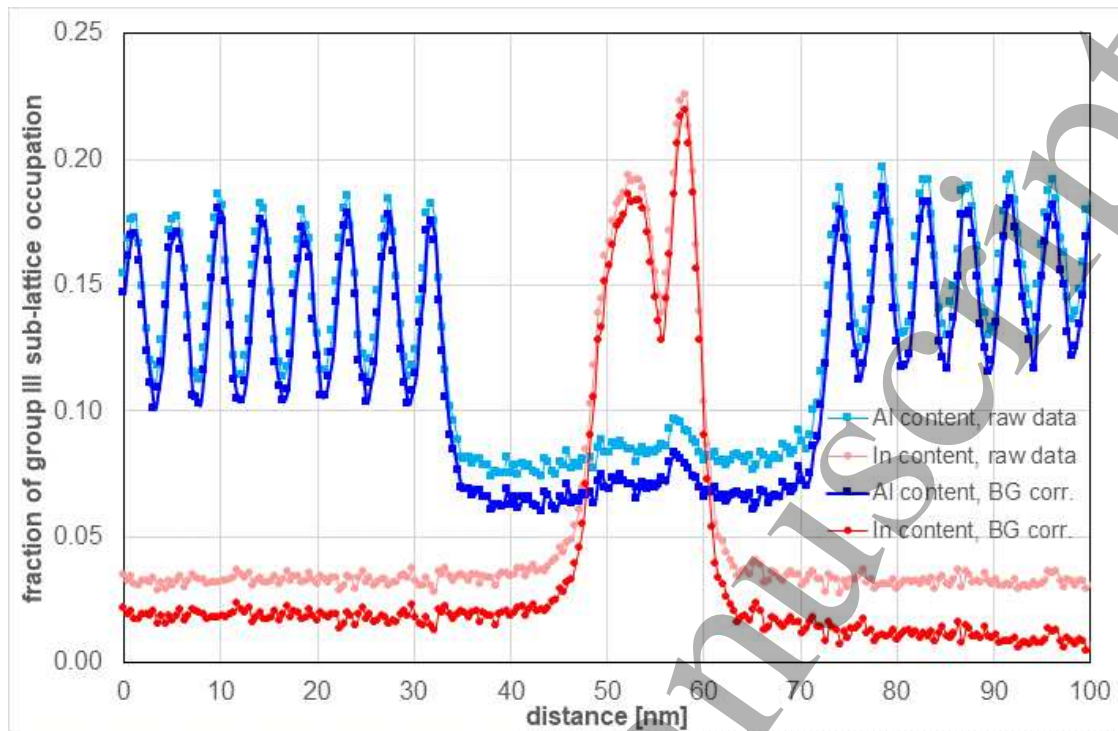


Figure 8: line profiles of the ratios of the raw X-ray maps of Al/(Al+Ga+In) and In/(Al+Ga+In) for sample A558. Again, a strong Al increase coincides with the start of the QD layer growth while perhaps a fainter signal is visible near the start of the QW layer underneath.

3. Result and discussion

A central problem of quantifying X-ray maps is low count rates due to short dwell times at individual pixels, even with larger and multiple X-ray detectors. Table 2 lists the statistics of the X-ray maps shown in figures 3 (sample A527) and 7 (sample A558).

sample	A527 ->				A558 ->					
element	X-ray line	min	max	mean	rms	min	max	mean	rms	type
C	K	7	53	26.6	±5.7	96	320	198.4	±28.3	?
O	K	0	13	2.7	±1.6	0	10	1.8	±1.4	?
Ne	K	0	14	3.5	±1.9	0	9	1.5	±1.2	n
Al	K	0	20	4.7	±2.5	0	32	9.5	±4.6	s
Si	K	0	15	3.5	±1.9	0	16	5.5	±2.8	n
Ar	K	0	9	1.5	±1.2	0	7	0.7	±0.8	?
Ti	K	0	9	1.3	±1.2	0	7	0.7	±0.8	n
Fe	K	0	9	1.5	±1.2	0	8	0.9	±0.9	n
Co	K	0	9	1.6	±1.3	0	8	0.8	±0.9	n
Cu	K	0	9	1.6	±1.3	0	8	0.8	±0.9	n
Ga	K	14	70	38.7	±6.6	24	112	61.8	±13.4	s
As	K	17	76	39.6	±6.4	20	112	60.5	±12.7	s
In	L	0	15	1.8	±1.6	0	32	3.8	±4.3	s

Table 2: statistics of counts of X-ray maps. rms= root mean square (standard deviation). Type: n=noise, s=true signal,?=possible signal due to surface contamination (C), oxidation (O) or argon incorporation due to ion milling (Ar)

In order to estimate the spatial resolution we have tried to determine the thickness more accurately combining two different approaches, one based on geometry and one based on analyzing spectral count rates, as follows: the areas investigated were about 160nm (A527) and 100nm (A558) away from the specimen edge. For a perfect 10° wedge geometry (as the ion beam impinged under 5° on both surfaces) this would give thickness estimates of 28.0nm and 17.5nm, respectively, but such perfect wedges can rarely be achieved. Often, samples are more rounded at the edges. The thickness *difference* between the two areas should however remain to be 10.5nm, even with rounded edges. From the spectra taken in succession without changing the electron beam current we can work out the X-ray count rates as 14114 s⁻¹ (A527) and 8385 s⁻¹ (A558) and can thus conclude that the thickness *ratio* should be 1.683:1, i.e. the second area has only 59.4% the thickness of the first. Combining this with the above information gives absolute thickness values of 25.9nm for A527 and 15.4nm for A558. Using the standard formulas for electron beam broadening [24, 25] then suggests beam broadening of 1.2nm for the 26nm thick area of sample A527 and 0.5-0.6nm for the 15.4nm thin area of A558. We have cross-checked this with previous Monte Carlo calculations of the Ga K/L line ratio for InGaAs samples using an ideal Si:Li detector with ultrathin polymer window as was appropriate for our JEOL 2010F [26]. For the windowless SDD detectors used here, the Ge L count rate will go up as a

~300nm thick carbon layer would no longer absorb ~18% of this X-ray line. At the same time the Ge K count rate will go down by ~2% because the silicon in SDD detectors has only the typical wafer thickness of 0.5mm so some hard X-rays can penetrate it. We can hence use previous plots of Ga K/L ratio vs thickness if we recalibrate the value for zero thickness to be 0.81 times the value of 1.20 for Si:Li, i.e. 0.97. The Ga K/L ratios we actually measured in our spectra of 0.973 and 1.027 would then suggest thicknesses of around 4nm and 28nm, respectively, which are in reasonable agreement with the above estimates, given the relative large errors of this approach.

We have then used Monte Carlo simulations [27] for 200keV electrons to further investigate X-ray generation, absorption, fluorescence and detection at a take-off angle of 25°.

Simulations of X-ray absorption for AlInGaAs samples at thicknesses of 16-28 nm show that no absorption correction needs to be included for Ga K and In L lines relative to As K, the only slightly affected X-ray being the softer Al K line whose intensity is expected to decrease by 7-8% and so would need an absorption correction factor of 1.07±0.02.

Mutual fluorescence that could increase the Al K line intensity has been studied by a series of simulations of X-ray generation on InGaAs samples of varying thickness with a thin AlAs layer in the centre sandwiched between GaAs at the bottom and either InAs or GaAs in the top half. We considered thicknesses from 10 to 600nm. We evaluated the fluorescence from the In L onto the Al K line by comparing the apparent increase in Al X-ray intensity when the GaAs overlayer was replaced by InAs and found that in the thickness range of 10-40nm relevant for our experiments the effect was hardly detectable (maximal 1.8% relative increase at 40nm for 16nm pure InAs on top) and so we conclude that mutual fluorescence is negligible in our samples that are very thin and wherein both the overall In and Al content are much lower.

This means that quantification can be performed using the standard thin-film approximation first used by Cliff and Lorimer [21]. For quantifying X-ray spectra from thin samples the intensities, I , of an individual line chosen for each element (index j) should be multiplied by their k -factors and, if these are calibrated for weight fractions, divided by the corresponding atomic weights A so that

$$x_j = \frac{I_j k_j / A_j}{\sum_n I_n k_n / A_n} \quad (\text{eqn. 1})$$

gives the concentration of element j in thin film approximation where the sum extends over all n elements. We have in the plots of figures 4 and 8 completely neglected k -factors because the scale factors k_j/A_j are all close to unity for the (Al,Ga,In)As system if the common As K-line (A_{SK}) is used for reference: from extrapolating Monte Carlo simulations for AlGaAs and InGaAs back to zero thickness, and taking into account the same modifications as before to replace a thick Si:Li with ultrathin polymer window by a windowless SDD detector, we get $k_{AlK,A_{SK}}=0.32\pm0.04$, $k_{GaK,A_{SK}}$

= 0.98 ± 0.01 [26] and $k_{\text{InL,AsK}} = 1.47 \pm 0.03$ [28]. Using the nominal k -factors of the JEOL supplied software instead would give $k_{\text{AlK,AsK}} = 0.359$, $k_{\text{GaK,AsK}} = 0.853$, $k_{\text{InL,AsK}} = 1.284$. The k -factors in equation (1) need to be divided by the atomic weights and then divided by $k_{\text{AsK}/A_{\text{As}}}$, i.e. the above values for $k_{j,\text{AsK}}$ need to be multiplied by the relative atomic weights A_{As}/A_j . The results are tabulated in Table 3.

model		CASINO		JEOL
element	X-ray line	A_j	$k_{j,\text{AsK}} \cdot 74.92/A_j$	
Al	K	26.98	0.883 ± 0.106	0.996
Ga	K	69.72	1.051 ± 0.011	0.916
In	L	114.8	0.961 ± 0.018	0.838

Table 3: k -factors of X-rays of group III elements (index j) relative to As K line, multiplied by A_{As}/A_j

This means the real Al and In content could have been a little lower than shown in the plots, but given the poor statistics and that the use of the above correction factors would only marginally improve the ratio of all group III elements to arsenic (which should yield unity but is always above that value), we decided to neglect this correction.

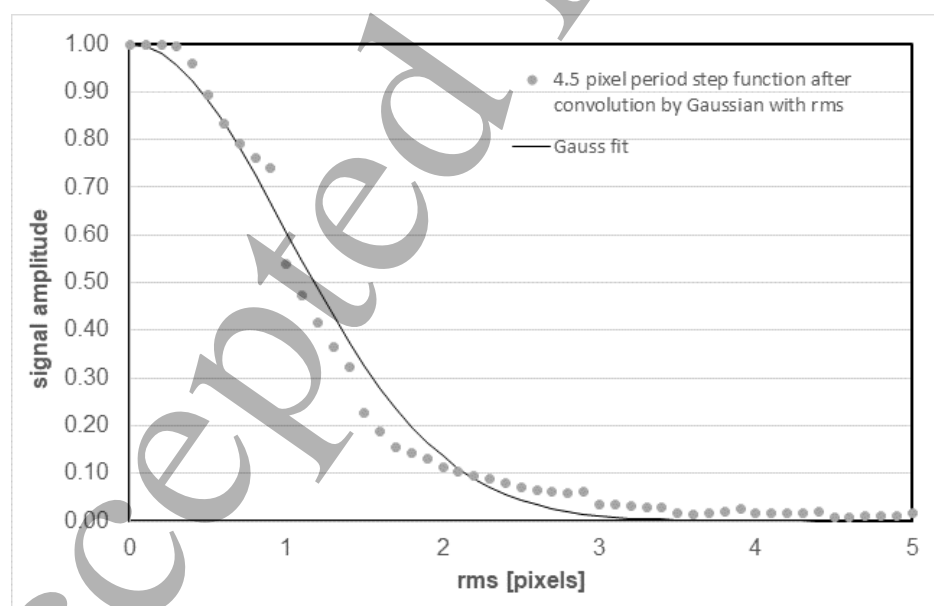


Figure 9: numerical simulation of the effect of resolution upon signal amplitude of a 4.5 pixel ideal 1D step function when convoluted with a 2D Gaussian of given root-mean-square (rms) value. For the AlGaAs/GaAs superlattice, set 1nm = 1pixel to

1
2
3 evaluate.

4
5
6 All linescans clearly reveal the shorter AlGaAs/GaAs superlattice (of period 4.5nm)
7 and the measured full widths at half maximum (FWHM) values of the narrowest
8 individual layers prove that the resolution must be 2nm or better in both cases.
9 Concerning the influence of resolution on the contrast of maps and linescans three
10 effects should be considered:
11

- 12 i) the sampling increment given by the effective pixel width, here 0.26nm in the
13 first and 0.39nm (after binning) in the second case;
- 14 ii) the impinging focused electron probe profile (here: 0.16nm FWHM, giving an
15 rms width of approximately $\sigma_p=0.07$ nm in Gaussian approximation);
- 16 iii) the broadening of the electron in the sample due to multiple elastic scattering,
17 as evaluated before.
18
19

20
21 While effect ii) will be negligible in our case (the above rms width corresponding to
22 only 0.18-0.26 pixels would dampen the signal from the superlattice by 6% at the
23 most, according to the plot in figure 9), electron beam scattering in iii) will dominate
24 the effective resolution. This can be shown by again evaluating models for electron
25 probe spreading, which for 15-26 nm thin GaAs ($\langle Z \rangle=32$, $\rho=5.32$ g cm⁻³, $U=200$ kV)
26 suggest $b=1.4$ nm for the 1.9σ beam diameter that contains 90% of intensity [29] (i.e.,
27 $\sigma_b=0.74$ nm) or $b=0.5-1.2$ nm for the full beam diameter at the exit surface [25]
28 (hence, $\sigma_b=0.2-0.5$ nm for an equivalent Gauss function). These values are larger than
29 the nominal probe σ_p and would dampen the apparent superlattice modulation of the
30 Al content by 10-20% of the nominal value of $\Delta y_{Al}^{nom}=0.33$, i.e bring it down to 0.26.
31 We measure, however, only an amplitude of $\Delta y_{Al}^{exp}=0.08$, which indicates that there
32 must be real interdiffusion of Al within the superlattices, corresponding to an rms
33 diffusion length for Al atoms of ~ 1.5 nm.
34
35
36
37
38

39
40 The peak indium concentrations x_{In} measured are also somewhat lower than the
41 nominal values (0.19 instead of 0.25 for the lower QW of sample A558, 0.12 [0.22]
42 for the QDs instead of 0.55 [0.60] for sample A527 [558]), which again indicates
43 some indium interdiffusion, but only over ~ 0.5 nm in length, in line with our
44 resolution estimate.
45
46

47
48 The concentration profiles from the group-III elements Al and In in figure 8 show
49 essentially the same features as before for the other specimen, but this time with
50 significantly higher In concentration (albeit still below the nominal values). The bump
51 in the Al profile correlates with the InGaAs QD layer, with their respective peaks
52 shifted by three pixels, or 1nm. The relative displacement of the In signal compared to
53 the Al signal by 0.5-1nm towards the top of the wafer structure indicates stronger
54 surface segregation of In compared to Al atoms. This finding for MBE growth of
55 (Al,In)GaAs differs from our previous findings for chemical vapour epitaxy of
56 (Al,In)GaN [30].
57
58
59
60

1
2
3 A key problem has been that the maps never gave zero base line values for elements
4 not in the sample. We therefore used the minimum experimental background found
5 for any element not in the sample (Ti K) to subtract 1.3 and 0.7 counts for the two
6 different samples. This worked well for the In L line but less so for the Al K line, and
7 we need to investigate further whether this problem is due to insufficient shielding to
8 stray X-rays (a possible collimator problem), the line fitting routine used (a software
9 problem) or simply due to the fact that all signals recorded are positive definite (i.e.
10 non-negative) maps that cut off small negative while retaining small positive values,
11 thereby skewing and offsetting the background by some artificial small amount.
12
13
14
15
16
17

18 **4. Conclusion**

19
20 X-ray maps have been quantitatively evaluated for all elements of the group-III sub-
21 lattice and direct evidence for 0.3-0.4 equivalent monolayers of Al deposited close to
22 the middle of the InGaAs quantum dots has been found.
23
24
25

26 **Acknowledgement**

27
28 We wish to acknowledge the Henry Royce Institute for Advanced Materials, funded
29 through EPSRC grants EP/R00661X/1, EP/S019367/1, EP/P02470X/1 and
30 EP/P025285/1, for the financial support for JN and for access to the JEOL JEM-F200.
31 E.-M Pavelescu acknowledges the PCCDI 75/2018 VARDIMTECH (PN-III-P1-1.2-
32 PCCDI -2017-0152) Project.
33
34
35
36
37
38

39 **References**

- 40
41 [1] H Bethe: Zur Theorie des Durchgangs schneller Korpuskularstrahlen durch
42 Materie. *Ann. Phys.* 397 (1930) 325-400.
43 [2] J Philibert: A method for calculating the absorption correction in electron-probe
44 microanalysis. *Proc. Int. Symp. X-ray Optics and X-ray Microanalysis*,
45 Academic Press, New York, ed HH Pattee, VE Cosslett and E Engström (1963)
46 p 379.
47 [3] SJB Reed: Characteristic fluorescence corrections in electron-probe
48 microanalysis. *Brit. J. Appl. Phys.* 16:7 (1965) 913-926.
49 [4] M Watanabe, Z Horita and M Nemoto: Absorption correction and thickness
50 determination using the zeta factor in quantitative X-ray microanalysis.
51 *Ultramicroscopy* 65:3-4 (1996) 187-198.
52 [5] T Walther: An improved approach to quantitative X-ray microanalysis in
53 (S)TEM: thickness dependent k -factors. *J. Phys. Conf. Ser.* 241 (2010) 012016.
54 [6] HS von Harrach, P Dona, B Freitag, H Soltau, A Niculae and M Rohde: An
55 integrated multiple silicon drift detector system for transmission electron
56 microscopes. *J. Phys. Conf. Ser.* 241 (2010) 012015.
57
58
59
60

- 1
2
3
4
5
6
7
8
9
10
11
12
13
14
15
16
17
18
19
20
21
22
23
24
25
26
27
28
29
30
31
32
33
34
35
36
37
38
39
40
41
42
43
44
45
46
47
48
49
50
51
52
53
54
55
56
57
58
59
60
- [7] LJ Allen, AJ D'Alfonso, B Freitag and DO Klenov: Chemical mapping at atomic resolution using energy-dispersive x-ray spectroscopy. *MRS Bulletin* 37:1 (2012) 47-52.
- [8] I Ohnishi, T Suzuki, K Miyatake, Y Jimbo, Y Iwasawa, M Morita, T Sasaki, H Sawada and E Okunishi: Analytical and in situ applications using aberration corrected scanning transmission electron microscope. *e-J. Surf. Sci. Technol.* 16 (2018) 286-288.
- [9] U Bangert, AJ Harvey, C Dieker, A Hartmann and R Keyse: Highly spatially resolved X-ray analysis of semiconductor alloys and nanostructures in a scanning transmission electron microscope. *Philos. Mag. A* 74:6 (1996) 1421-1437.
- [10] D Zhi, H Davock, R Murray, C Roberts, TS Jones, DW Pashely, PJ Goodhew and BA Joyce: Quantitative compositional analysis of InAs/GaAs quantum dots by scanning transmission electron microscopy. *J. Appl. Phys.* 89:4 (2001) 2079-2083.
- [11] T Walther: Comparison of experimental and theoretical X-ray intensities from (In)GaAs specimens investigated by energy-dispersive X-ray spectroscopy in a transmission electron microscope. *J. Phys. Conf. Ser.* 209 (2010) 012029.
- [12] H Amari, L Lari, HY Zhang, L Geelhaar, C Cheze, MJ Kappers, C McAleese, CJ Humphreys and T Walther: Accurate calibration for the quantification of the Al content in AlGaIn epitaxial layers by energy-dispersive X-ray spectroscopy in a Transmission Electron Microscope. *J. Phys. Conf. Ser.* 326 (2011) 012018.
- [13] H Bender, F Seidel, P Favia, O Richard and W Vandervorst: X-ray absorption in pillar-shaped transmission electron microscopy specimens. *Ultramicroscopy* 177 (2017) 58-68.
- [14] JS Kim, PW Yu, JY Leem, JI Lee, SK Noh, JS Kim, SM Kim, JS Son, UH Lee, YS Yim, D Lee: Energy level control of self-assembled InAs quantum dots utilizing an thin AlAs layer. *Appl. Phys. Lett.* 78: 21 (2001) 3247-3249.
- [15] YQ Wei, SM Wang, F Ferdos, J Vukusic, QX Zhao, M Sadeghi, A Larsson: Aluminium incorporation for growth optimization of 1.3 μ m emission InAs/GaAs quantum dots by molecular beam epitaxy. *J. Cryst. Growth* 215 (2003) 172-176.
- [16] F Ferdos, S Wang, Y Wei, M Sadeghi, Q Zhao, A Larsson: Influence of initial GaAs and AlAs cap layers on InAs quantum dots grown by molecular beam epitaxy. *J. Cryst. Growth* 251 (2003) 145-149.
- [17] SI Jung, JJ Yoon, HJ Park, YM Park, MH Jeon, JY Leem, CM Lee, ET Cho, JI Lee, JS Kim, JS Son, JS Kim, DY Lee, IK Han: Bandgap engineering of self-assembled InAs quantum dots with a thin AlAs barrier. *Physica E* 26 (2005) 100-104.
- [18] SJ Pennycook and DE Jesson: High-resolution Z-contrast imaging of crystals. *Ultramicroscopy* 37 (1991) 14-38.
- [19] Y Qiu, L Lari, IM Ross and T Walther: Comparison of the contrast in conventional and lattice resolved ADF STEM images of InGaAs/GaAs structures using different camera lengths. Proc. MSM-17, Cambridge, UK. *J.*

- 1
2
3
4
5
6
7
8
9
10
11
12
13
14
15
16
17
18
19
20
21
22
23
24
25
26
27
28
29
30
31
32
33
34
35
36
37
38
39
40
41
42
43
44
45
46
47
48
49
50
51
52
53
54
55
56
57
58
59
60
- Phys Conf. Ser.* 326 (2011) 012041.
- [20] T Walther: A new experimental procedure to quantify annular dark field images in scanning transmission electron microscopy, *J. Microsc.* 221 (2006) 137-144.
- [21] G Cliff and GW Lorimer: Quantitative analysis of thin specimens. *J. Microsc.* 103: 3 (1975) 203-207.
- [22] X Wang, J Bai and T Walther: Self-consistent absorption correction for quantification of the indium and aluminium content from noisy X-ray maps of group III nitride nanowires. *J. Microsc.* 272:2 (2018) 111-122.
- [23] T Walther, AG Cullis, DJ Norris and M Hopkinson: Nature of the Stranski-Krastanow transition during epitaxy of InGaAs on GaAs. *Phys. Rev. Lett.* 86 (2001) 2381-2384.
- [24] DB Williams and CB Carter: *Transmission Electron Microscopy. IV Spectrometry*. Springer, New York, 1996.
- [25] T Walther: Development of a new analytical electron microscopy technique to quantify the chemistry of planar defects and to measure accurately solute segregation to grain boundaries. *J. Microsc.* 215:2 (2004) 191-202.
- [26] T Walther and X Wang: Self-consistent method for quantifying indium content from X-ray spectra of thick compound semiconductor specimens in a transmission electron microscope, *J. Microsc.* 262:2 (2016) 151-156.
- [27] D Drouin, AR Couture, D Joly, X Tastet, Y Aimez and R Gauvin: CASINO v2.42. – a fast and easy-to-use modeling tool for scanning electron microscopy and microanalysis users. *Scanning* 29:3 (2007) 92-101.
- [28] MC Parri, Y Qiu and T Walther: New pathways for improved quantification of energy-dispersive X-ray spectra of semiconductors with multiple X-ray lines from thin foils investigated in transmission electron microscopy. *J. Microsc.* 260: 3 (2015) 427-441.
- [29] JI Goldstein, JL Costley, GW Lorimer and SJB Reed: Quantitative X-ray analysis in the electron microscope. In: Proc. Anal. Electr. Microsc., Chicago, *Scanning Electron Microscopy* 1 (1977) 315-324.
- [30] T Walther, H Amari, IM Ross, T Wang and AG Cullis: Lattice resolved annular dark-field scanning transmission electron microscopy of (Al,In)GaN/GaN layers for measuring segregation with sub-monolayer precision. *J. Mater. Sci.* 48 (2013) 2883-2892.